Supporting Information

Self-assembly of polyoxovanadate-capped polyoxoniobates and their catalytic decontamination for sulfur mustard simulant

Ni Zhen, Jing Dong, Zhengguo Lin, Xiaoxia Li, Yingnan Chi* and Changwen Hu

Key Laboratory of Cluster Science of Ministry of Education, Beijing Key Laboratory of Photoelectronic/Electrophotonic Conversion Materials, School of Chemistry and Chemical Engineering, Beijing Institute of Technology, Beijing, P. R. China. E-mail: chiyingnan7887@bit.edu.cn.

1. Materials and Methods

All reagents and solvents for the syntheses were purchased from commercial sources and used as received, excepted for $K_7HNb_6O_{19}\cdot 13H_2O$, which was prepared according to the literature [1] and its identity was confirmed by IR spectrum. Elemental analyses (K, Na, Cs, V, Nb) were determined with a Thermo ICP atomic emission spectrometer; C, H, N were determined by an ElementarVario EL cube Elmer CHN elemental analyzer. Powder X-ray Diffraction (PXRD) was performed on SHIMADZU XRD-6000 X-ray diffractometer equipped with graphite monochromatized Cu Kα radiation (λ = 0.154056 nm). X-ray photoelectron spectrum (XPS) analysis was conducted on a Thermo ESCALAB 250Xi spectrometer using an Al Kα radiation as the X-ray source (1486.6 eV) with a pass energy of 30 eV and the pressure inside the analyzer was maintained at 10^{-9} Torr. IR spectra were recorded on a Bruker FT-IR spectrophotometer (KBr pellets) over the region of 400-4000 cm^{-1}. Thermogravimetric analyses (TGA) were performed on a LABSYS EVO analyzer heated from 25 °C to 800 °C under a nitrogen gas atmosphere with a heating rate of 10 °C·min^{-1}. Scanning electron microscopy (JEOLS-4800) and transmission electron microscopy (JEOL JEM-2010) were used to observe the morphology and microstructure of the samples before and after catalytic reactions. The Raman spectra were obtained on LabRam HR800 with an excitation wavelength of 633 nm. The GC analyses were performed on Shimadzu GC-2014C with a FID detector equipped and an HP-5 ms capillary column. The GC-MS spectra were obtained using an Agilent 7890A-5975C instrument at an ionization voltage of 1200V.

2. Catalytic oxidation of 2-chloroethyl ethyl sulfide (CEES)

The selective oxidation (decontamination) of CEES using different catalysts (V_5Nb_{23}, V_6Nb_{23} and $V_{3.5}Nb_{24}$) were performed as follows. Catalyst (crystal samples, 6.47×10^{-4} mmol) was dispersed in acetonitrile (3 mL) and to this solution CEES (0.4 mmol) and 1,3-dichlorobenzene (internal standard, 0.2 mmol) were added. After stirring for 2 minutes at room temperature, 3% aqueous H_2O_2 (0.44 mmol) was added dropwise. The reaction was monitored by gas chromatography at various time intervals and the products were qualitatively analyzed by GC-MS. **CAUTION**: The simulant of CWAs (CEES) is highly toxic and must be handled only by trained personnel using applicable safety procedures in a closed system or in a hood under good ventilation.

Leaching test: The catalyst was filtered off from the reaction mixture after 30 min and the solution was kept running under the same conditions for another 30 min. The reaction was monitored by gas chromatography at various time intervals.

3. Synthesis

Synthesis of 1. The mixture of $K_7HNb_6O_{19}\cdot 13H_2O$ (0.706 g, 0.52 mmol), $NaVO_3$ (0.0756 g, 0.62 mmol), $NaHCO_3$ (0.3 g, 3.57 mmol), Tris (0.156-0.624 g, 1.29-5.15 mmol) and CsCl (0.226 g, 1.34 mmol) in 8 mL water was put in a 23 mL Teflon-lined autoclave, which was sealed and heated at 180 °C for 3 days. After slowly cooling to room temperature, a clear solution was obtained, filtered and evaporated at room temperature. The resulting brown-block crystals were obtained after three weeks. Yield: 1.58% based on $NaVO_3$. Anal. Calc: Nb, 41.88; V, 4.99; Cs, 10.42; K, 5.36; Na, 2.25. Found: Nb, 42.34; V, 4.93; Cs, 12.41; K, 5.33; Na, 2.14. IR (KBr disks): 508, 665, 814, 872, 956 cm^{-1}.

Synthesis of 2. Compound **2** was prepared following the procedure described for **1**, but slow diffusion of ethyl acetate into the reaction solution was used instead of evaporation. Yield: 2.68% based on $NaVO_3$. Anal. Calc: Nb, 40.06; V, 5.73; Cs, 9.97; K, 5.86; Na, 2.15. Found: Nb, 40.56; V, 5.60; Cs, 8.63; K, 5.73; Na, 2.13. IR (KBr disks): 508, 662, 815, 882, 964 cm^{-1}.

Synthetic discussion. We systematically explored the effects of synthetic parameters on the synthesis for compounds **1** and **2**, including pH (10.0-12.5), Nb:V ratio (from 2:1 to 6:1), temperature (100 ℃-190 ℃), and the amount of Tris. The experimental results showed that the amount of Tris was a vital for the isolation of title compounds. Although the reproducibility of experiments is obviously enhanced by adding additional Tris (four to six times the original amount) to the hydrothermal reaction solution, but the synthetic yield was still unsatisfactory. The main reason is that the soluble Nb precursors tend to form amorphous precipitation in aqueous solution. In addition, classic Keggin structure $\{VNb_{12}O_{40}(VO)_2\}$ or reported $\{V_{3.5}Nb_{24}\}$ as main product was obtained during the crystallization process. For example, when the mother liquor that generates $\{V_5Nb_{23}\}$ was filtered, the further evaporation gave rise to a large amount of $\{V_{3.5}Nb_{24}\}$ and after the isolation of $\{V_6Nb_{23}\}$, the crystals of Keggin-type $\{VNb_{12}O_{40}(VO)_2\}$ were generated.

4. X-ray Crystallography

The intensity data of the compounds were collected on a Bruker Apex CCD II area-detector diffractometer with graphite-monochromated Mo Kα radiation (λ = 0.71073 Å) at 153(2) K. Absorption corrections were applied using multiscan techniques. Their structures were solved by direct methods and refined by full-matrix least-squares techniques using the SHELXL-2016/6 program [2-4]. Crystallographic data for compounds **1**-**2** is summarized in Table S1. The bond length (Å) and angle (deg) range of compounds **1**-**2** are listed in Table S2. BVS results for compounds **1** and **2** are listed

in Table S3. The crystallographic data have been deposited with the Cambridge Crystallographic Data Centre (CCDC) as entries 2006353 (**1**), 2006356 (**2**).

NOTE: (1) The calculated formulas is based on Z = 1, namely, there is one POM molecule in the unit cell. However, according to structural analysis, there are four discrete PONb clusters in the unit cell of compound **1** and two discrete PONb clusters in the unit cell of compound **2**, respectively. In addition, according to the single crystal X-ray diffraction data, it seems not all the crystal water and cations can be modeled with accurate location due to the weak diffraction, which is very common in POM chemistry. There are some residual disordered or partial-occupied water and cations are not located in the cif file. The final molecular formula was defined by SXRD data combined with elemental analysis, which is the reason why the calculated Mol. weight and Mu Ratio differs from reported ones. As a result, the density is different, too. (2) Residual density might be caused by some residual disordered or partial-occupied water and cations in the compounds, but it will not affect the core structure of the POM; (3) A cavity with a diameter of about 4 Å is formed by the linkage of lacunary $\mathbf{Nb_{23}}$ and capping $\mathbf{V_5/V_6}$, which was occupied with solvent molecules or counter cations. However, their disordered arrangement made it difficult to be further determined; (4) It seems to be very difficult to model all the H atoms on water molecules in the two compounds due to the distinct diffraction difference between the heavy Nb atoms and light H atoms. Because the locations of most these hydrogen atoms are still not very accurate based on the current diffraction data (Mo Kα source), the hydrogen atoms on waters were not incorporated in the refinement. The final molecular formula was defined by SXRD data combined with elemental analysis.

Table S1. Crystal data and structure refinement for compounds **1** and **2**.

	1	**2**
Empirical Formula	$Cs_4H_{62}K_7Na_5V_5Nb_{23}O_{108}$	$Cs_4H_{74}K_8Na_5V_6Nb_{23}O_{115}$
Fw ($g \cdot mol^{-1}$)	5102.41	5316.55
T (K)	153(2)	153(2)
Radiation (λ, Å)	0.71073	0.71073
Crystal system	Monoclinic	Monoclinic
Space group	P2(1)/c	P2(1)/m
a (Å)	14.9822(11)	15.9678(8)
b (Å)	25.2721(18)	23.5105(13)
c (Å)	31.619(2)	16.2976(9)
α (°)	90	90
β (°)	93.655(2)	104.3296(16)
γ (°)	90	90
V ($Å^3$)	11947.6(15)	5927.9(6)
Z	4	2
$d_{calcd.}$ $Mg \cdot m^{-3}$	2.837	2.979
μ, mm^{-1}	4.057	4.206
GOF	1.099	1.030
Final R indices	R_1[a] = 0.0886	R_1[a] = 0.0609
[R>2σ(I)]	wR_2[b] = 0.2320	wR_2^b = 0.2062
R indices (all data)	R_1^a = 0.0982	R_1[a] = 0.0710
	wR_2^b = 0.2397	wR_2[b] = 0.2196

[a] $R1 = \Sigma||F_0| - |F_c|| / \Sigma|F_0|$;

[b] $wR2 = \Sigma[w(F_0^2\text{-}F_c^2)^2]/ \Sigma[w(F_0^2)^2]^{1/2}$

Table S2. The bond length (Å) and angle (deg) range in compounds **1** and **2**.

Bond	**1**	**2**
Nb-O_t	1.727-2.387	1.706-2.379
V-O_t	1.592-1.626	1.601-1.711
Nb-O_{b1}	1.814-2.344	1.796-2.372
V-O_{b1}	1.786-1.850	—
Nb-O_{b2}	1.879-2.411	1.884-2.371
V-O_{b3}	1.924-1.948	1.910-1.960
Nb-O_c	1.933-2.392	1.929-2.372
Angle	**1**	**2**
Nb-O_{b1}-Nb	107.26-153.16	107.55-151.34
Nb-O_{b2}-Nb	90.52-143.01	91.64-141.63
V-O_{b3}-V	140.96-146.29	96.32-147.09
Nb-O_c-Nb	90.98-153.61	90.21-155.17
O_t	t=terminal oxygen, bonded to one Nb or one V	
O_{b1}	b_1=bridging oxygen, bonded to two Nb atoms or two V atoms	
O_{b2}	b_2=bridging oxygen, bonded to three Nb atoms	
O_{b3}	b_3=bridging oxygen, bonded to two V atoms and one Nb atom	
O_c	c=central oxygen, bonded to four Nb atoms	

Table S3. BVS results of V atoms for compounds **1** and **2**.

	V1	V2	V3	V4	V5	V6
Compound **1**	4.86	4.29	4.99	4.26	4.94	—
Compound **2**	4.40	4.15	4.11	4.15	4.11	3.85

Table S4. Comparison of the heterogeneous catalysts for the oxidative decontamination of sulfur mustard simulant.

catalyst	oxidant	TON[c]	TOF (min^{-1})[d]	conv. (%)	Sulfoxide selectivity (%)	ref.
compound **1**	3% H_2O_2	587.3	9.8[e]	95	> 96	this work
compound **2**	3% H_2O_2	612.1	10.2[e]	> 99	> 96	this work
Mg_3Al-LDH-Nb_6	3% H_2O_2	287.4	2.4[j]	95	96	5
Nb_2O_5	30% H_2O_2	186.7	0.6[f]	> 99	73	6
PV_2Mo_{10}/carbon	TBHP	124.3	—	100	—	7
$CoAsMo_6$[a]	30% H_2O_2	65.7	13.1[g]	98.5	> 99.9	8
Nb-SAP[b]	30% H_2O_2	46.7	0.1[h]	> 98	73	9
PW_{12}@NU-1000	30% H_2O_2	20.8	10.4[i]	98	57	10

[a]$CoAsMo_6$: $K_2H[(H_2O)_4Co][AsMo_6O_{21}(Ala)(PHBA)_2]\cdot 6.5H_2O$. [b]Nb-SAP: Niobium(V) Saponite Clay. [c]TON = moles product / moles of total catalytic clusters. [d]TOF = moles product / (moles of total catalytic clusters × amount of time). [e]Time = 60 min. [f]Time = 300 min. [g]Time = 5 min. [h]Time = 480 min. [i]Time = 2 min, [j]Time = 120 min.

To compare the catalytic activity of title compounds with the reported heterogeneous catalysts, especially POM-based heterogeneous catalysts, the type of oxidant, TON, TOF, conversion of sulfur mustard simulant, and selectivity for sulfoxide product are summarized and compared in Table S4. The selectivity (above 96%) for CEESO was achieved by **V_5Nb_{23}** and **V_6Nb_{23}**, which is much higher than most of the reported heterogeneous catalysts including Nb_2O_5 (selectivity: 73%, oxidant: 30% H_2O_2), Nb-SAP (selectivity: 73%, oxidant: 30% H_2O_2), and PW_{12}@NU-1000 (selectivity: 57%, oxidant: 30% H_2O_2). In addition, high turnover number (TON) was achieved by using nearly stoichiometric 3% aqueous H_2O_2. The TON of compound **1** (587.3) and **2** (612.1) are much higher than that of $CoAsMo_6$ (TON: 65.7, oxidant: 30% H_2O_2) and Mg_3Al-LDH-Nb_6 (TON: 287.4, oxidant: 3% H_2O_2).

By comparing the catalytic activity and structures of $\{V_5Nb_{23}\}$ (conversion: 95%, selectivity: 92%), $\{V_6Nb_{23}\}$ (conversion: 99%, selectivity: 96%), and $\{V_{3.5}Nb_{24}\}$ (conversion: 30%, selectivity: 82%) together with previous investigations, we think that both exposed Nb and V sites in POMs can contribute to the oxidation of CESS, but in vanadoniobates the exposed V sites are more active than Nb sites. For example, in $\{V_{3.5}Nb_{24}\}$ the V centres are surrounded by Nb and resultingly only the Nb sites can interact with H_2O_2 to form Nb-peroxo species, which is responsible for the oxidation of CEES. As for $\{V_5Nb_{23}\}$ and $\{V_6Nb_{23}\}$, both V and Nb centre are exposed and can interact with H_2O_2 to form Nb/V-peroxo species. As the catalytic activities of $\{V_5Nb_{23}\}$ and $\{V_6Nb_{23}\}$ are much better than that of $\{V_{3.5}Nb_{24}\}$, we conclude that the V sites is the main catalytic active sites in the title compounds. In addition, the formation of peroxo species in $\{V_5Nb_{23}\}$ and $\{V_{3.5}Nb_{24}\}$ was confirmed by the Raman spectra (Fig. S20), where a new peak at 868 cm^{-1} for $\{V_5Nb_{23}\}$ and 871 $cm^{-1}$for $\{V_{3.5}Nb_{24}\}$ assigned to O-O stretch were observed after treating with H_2O_2.

The high selectivity for CEESO over $CEESO_2$ might be related to the following three factors: (1) Based on previous investigation, we think that polyoxovanadates or polyoxoniobates have inherent advantage in the selective oxidation of sulfur mustard simulant when using H_2O_2 as oxidant; (2) 1.1 equivalent H_2O_2 as oxidant was used, which prevents the over oxidation in some degree; (3) According to the previous mechanism study,[11] CEES is oxidized by a two-step process: CEES was initially oxidized to the sulfoxide (CEESO) and the formed CEESO was further oxidized to sulfone ($CEESO_2$). The oxidation of the sulfide is faster than the sulfoxide, because the nucleophilicity of sulfur atom is reduced in the sulfoxide.

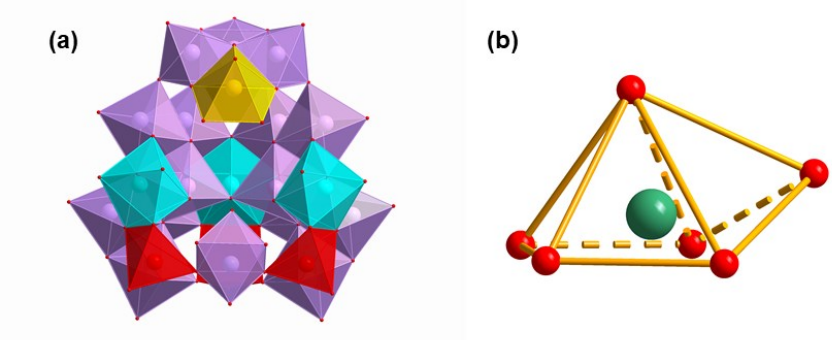

Fig. S1. (a) The coordination geometry of Nb centers in $\{Nb_{23}\}$. The octahedral $\{NbO_6\}$, pentagonal pyramidal $\{NbO_6\}$, pentagonal bipyramidal $\{NbO_7\}$ and square-pyramidal $\{NbO_5\}$ are presented as purple, yellow, blue and red polyhedra respectively. (b) The configuration of distorted pentagonal pyramidal $\{NbO_6\}$.

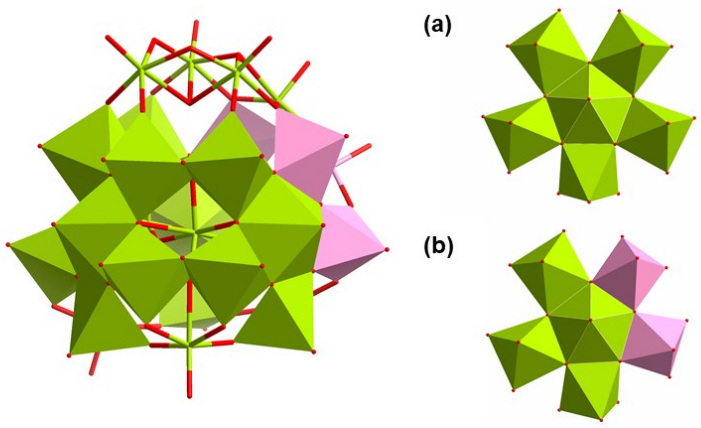

Fig. S2. Representation of the $\{Nb(Nb)_5\}$ (a) and $\{Nb(Nb)_3(V)_2\}$ (b) units in $\{V_5Nb_{23}\}$.

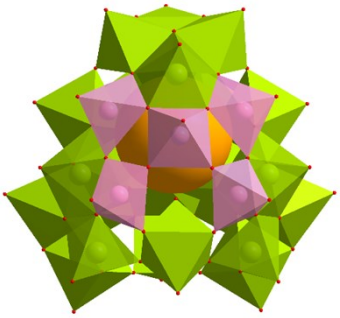

Fig. S3. View of the cavity in $\{V_5Nb_{23}\}$.

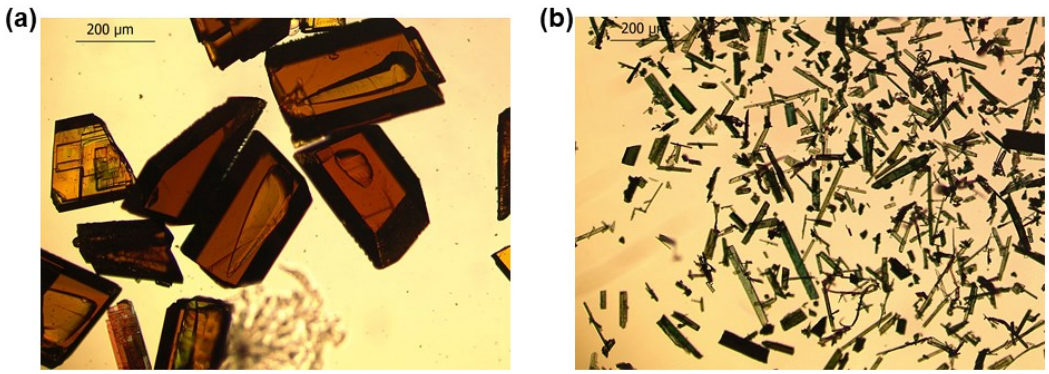

Fig. S4. Digital photographs of **1** (a) and **2** (b).

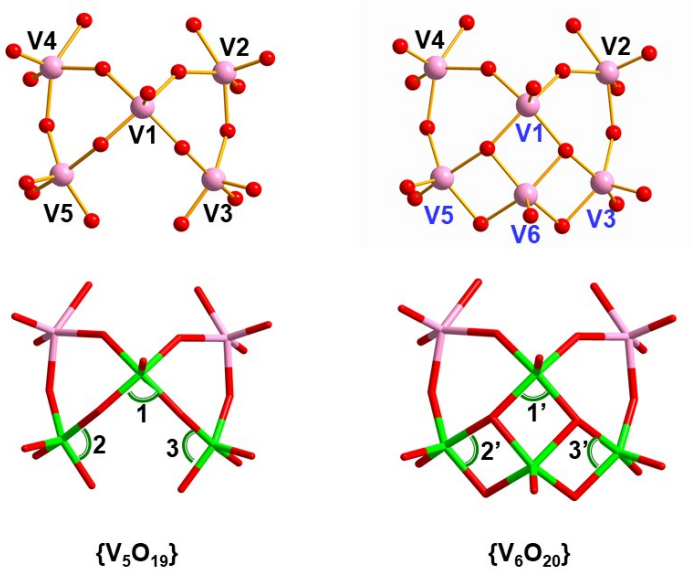

Fig. S5. The structural relationship between $\{V_5O_{19}\}$ in $\{V_5Nb_{23}\}$ and $\{V_6O_{20}\}$ in $\{V_6Nb_{23}\}$.

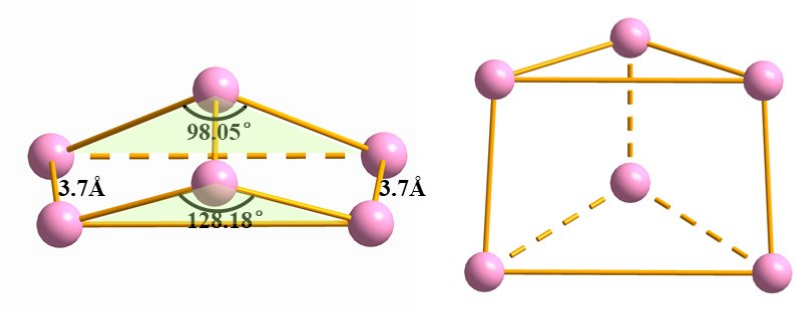

Fig. S6. An illustration of arrangement between the six V atoms in $\{V_6Nb_{23}\}$ along different axis.

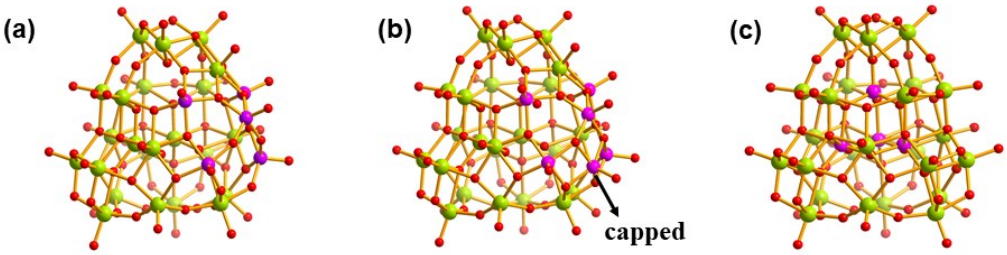

Fig. S7. Ball-and-stick presentations of $\{V_5Nb_{23}\}$ (a), $\{V_6Nb_{23}\}$ (b) and $\{V_{3.5}Nb_{24}\}$ (c), respectively.

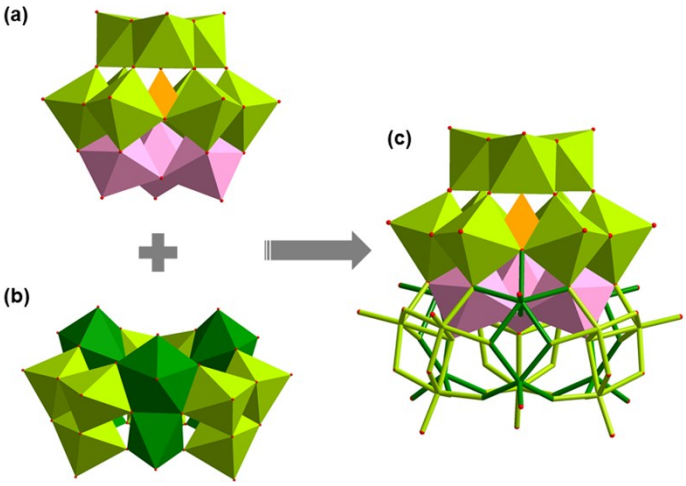

Fig. S8. Representations of $\{VNb_9V_{2.5}\}$ (a substituted V with half occupancy) (a), $\{Nb_{15}\}$ (b) and $\{V_{3.5}Nb_{24}\}$ (c) (NbO_6: pale green; NbO_5/NbO_7: green; VO_4: orange; VO_6: pink).

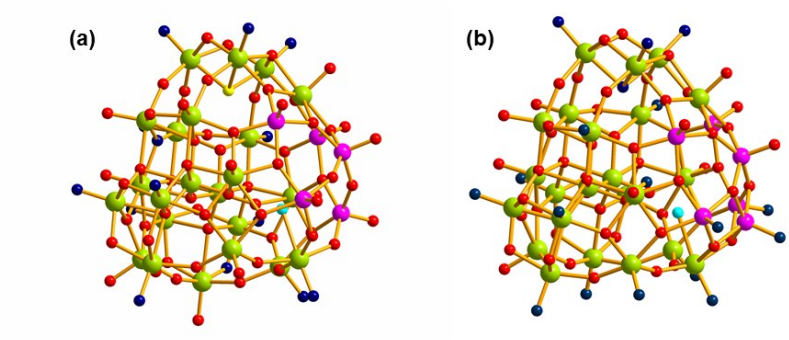

Fig. S9. BVS assignments of O atoms in **1** and **2**. All alkali metal ions are determined by a combination of X-ray diffractions and ICP analyses. Besides the alkali metal ions, 6 protons should be added to balance the charges of **1** and **2**. For **1**, bond valence sum (Σs) reveal that the oxidation states of 64 of 80 O atoms in $H_3Cs_4Na_5K_7[H_3V_5Nb_{23}O_{80}]$ (**1**) are -2 (-2.12 < Σs < -1.52, marked in red), 1 O atom at the center trivacant Keggin-type $\{Nb_9\}$ has a BVS value of 0.95 (marked in yellow), indicating it's protonated, 1 O atom is assigned as water ligand whose Σs value is 0.28 (marked in turquoise), and the Σs values of 14 O atoms are in the range of -1.31- -1.27 (marked in dark blue), indicating the three H^+ atoms are most likely delocalized on the 14 O atoms. For **2**, bond valence sum (Σs) reveal that the oxidation states of 62 of 81 O atoms in $H_4Cs_4Na_5K_8[H_2V_6Nb_{23}O_{81}]$ (**2**) are -2 (-2.10 < Σs < -1.50, marked in red), 1 O atom is assigned as water ligand whose Σs value is 0.28 (marked in turquoise), the Σs values of 18 O atoms are in the range of -1.46- -1.22 (marked in dark blue), indicating the four H^+ atoms are most likely delocalized on the 18 O atoms.[12]

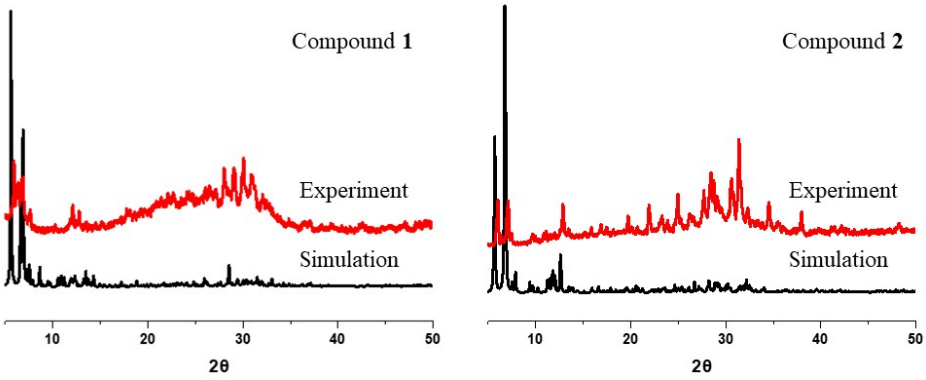

Fig. S10. The experimental (red) and simulated (black) PXRD patterns for compounds **1-2**, respectively. The main diffraction peaks of experimental patterns basically match with the simulated ones, confirming the crystal phase purity of compounds **1-2**.

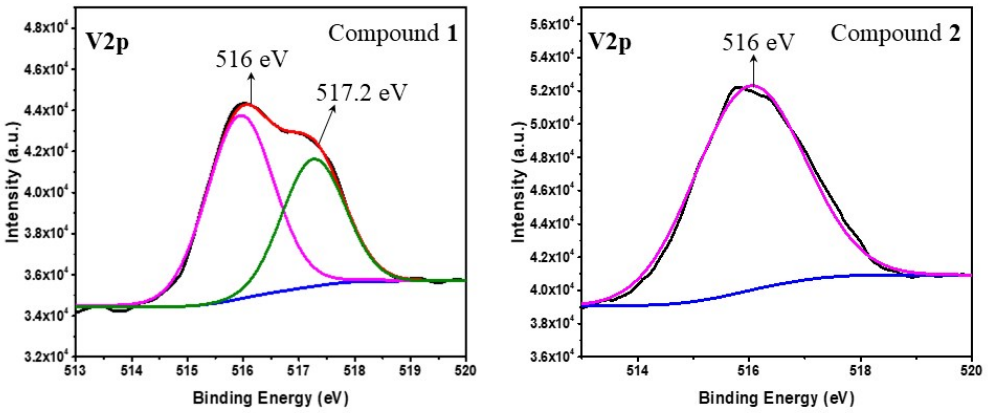

Fig. S11. The XPS spectrum of **1** gives two peaks at 517.2 and 516 eV, which should be attributed to V^{5+} $2p_{3/2}$ and V^{4+} $2p_{3/2}$, [13,14] respectively. The XPS spectrum of **2** gives one peak at 516 eV, corresponding to V^{4+} $2p_{3/2}$. [13]

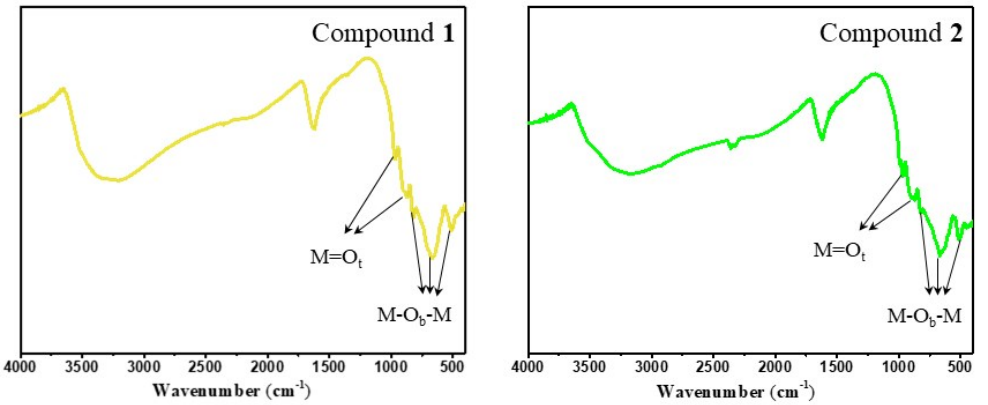

Fig. S12. The IR spectra of **1** and **2** recorded between 400 and 4000 cm^{-1}. The terminal $M=O_t$ (M = Nb, V) vibrations appear at 956 and 872 cm^{-1} for **1**, and at 964 and 882 cm^{-1} for **2**, respectively. [15-17] The characteristic peaks at 814, 665, and 508 cm^{-1} of **1** and 815, 662, and 508 cm^{-1} of **2** are assigned to the $\nu(M\text{-}O_b\text{-}M)$ stretches. [16,17] A peak around 1620 cm^{-1} can be seen in all the PONb spectra, which can be assigned to H_2O bending mode. The broad bands at around 3258 cm^{-1} of **1** and 3180 cm^{-1} of **2** are assigned to the vibration of water molecules.

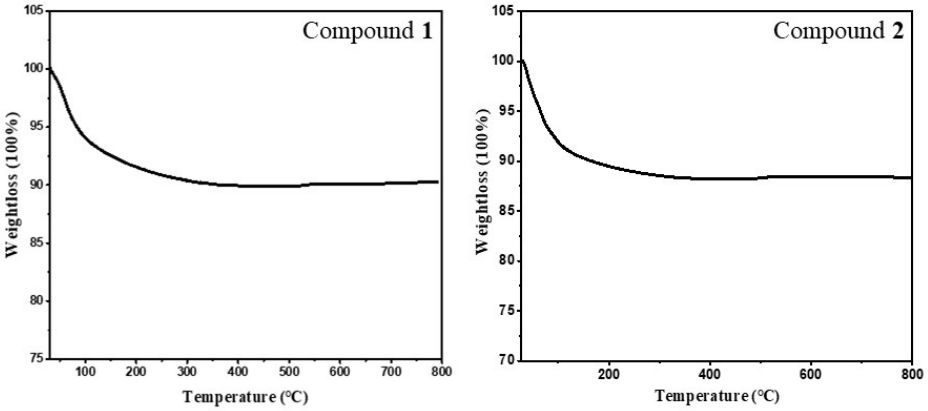

Fig. S13. The TG curves of **1** and **2**. The TG curve of **1** exhibits one step of weight loss, giving a total loss of 10.11% (calcd.10.23%) in the range of 25-300 °C. The weight loss is attributed to the removal of 28 crystal waters and one coordinated water molecule. Compound **2** undergoes one slow step of weight loss. The weight loss of 11.64% (calcd.11.85%) in the range of 25-300 °C is ascribed to the removal of 34 crystal waters and one coordinated water molecule.

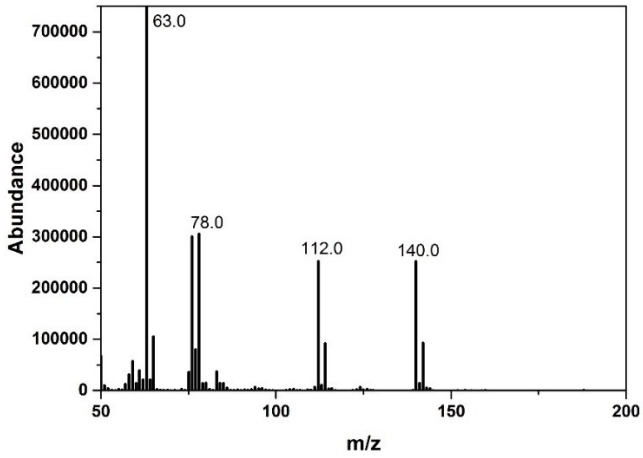

Fig. S14. Mass spectrum of 2-chloroethyl ethyl sulfoxide (CEESO).

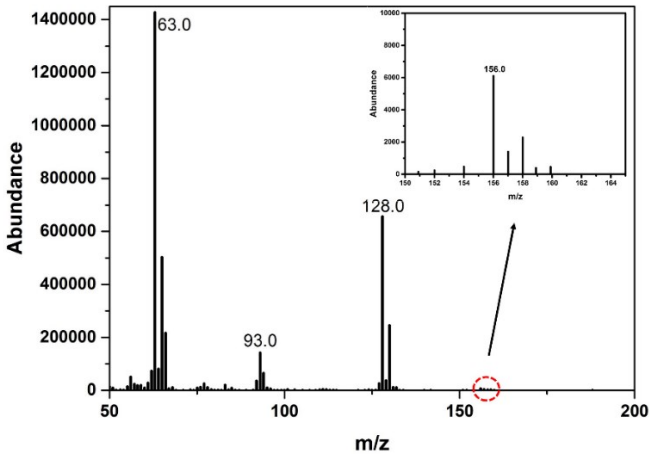

Fig. S15. Mass spectrum of 2-chloroethyl ethyl sulfone ($CEESO_2$).

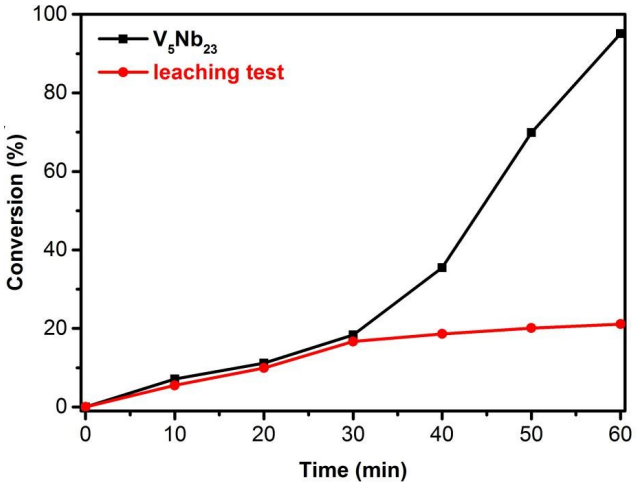

Fig. S16. The leaching test result. The oxidation of CEES over time using $\{V_5Nb_{23}\}$ (black); the catalyst was filtered off from the reaction mixture after 30 min and the solution was kept running under the same conditions for another 30 min (red). Reaction conditions: CEES (0.4 mmol), $\{V_5Nb_{23}\}$ (6.47×10^{-4} mmol), 1,3-dichlorobenzene (internal standard, 0.2 mmol), 3% aqueous H_2O_2 (0.44 mmol) and acetonitrile (3 mL) at room temperature.

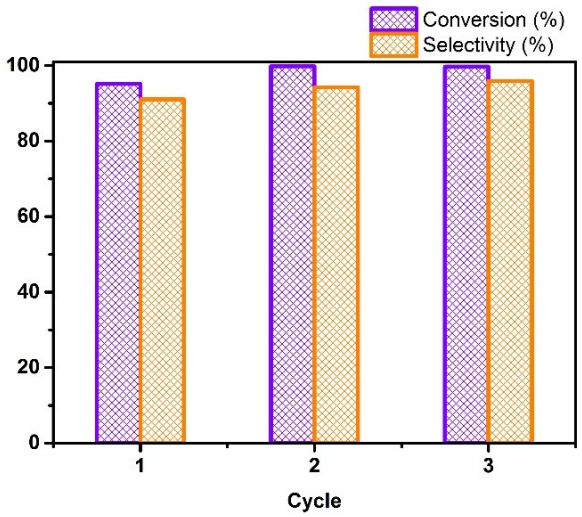

Fig. S17. Recycle test of compound **1** in the oxidative degradation of CEES.

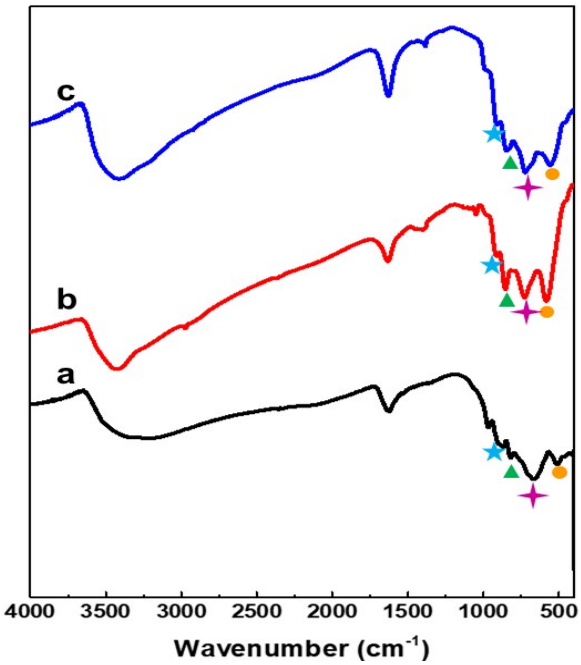

Fig. S18. The FT-IR spectra for (a) as-synthesized compound **1** and recovered catalyst after 1 catalytic run (b) and 3 catalytic run (c).

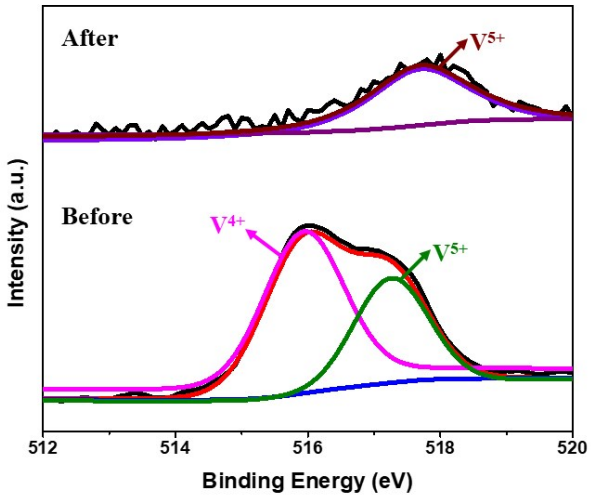

Fig. S19. The XPS spectra of **1** before and after the catalytic reaction, indicating that all the low-valent (+4) vanadium sites in the catalyst are oxidized to +5 under the turnover conditions.

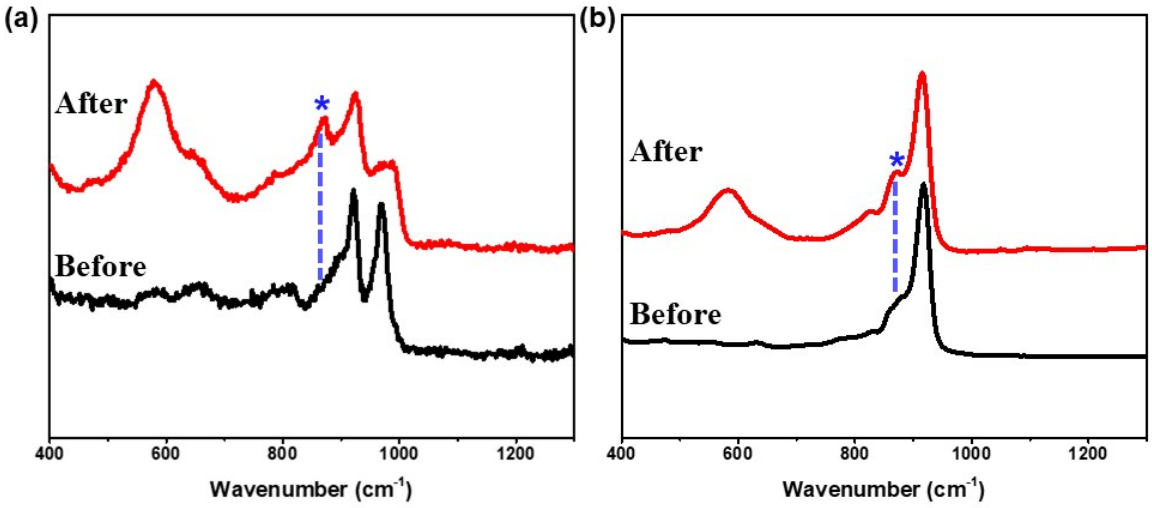

Fig. S20. (a) Raman spectra of **1** before and after treating with 30% H_2O_2; (b) Raman spectra of $\{V_{3.5}Nb_{24}\}$ before and after treating with 30% H_2O_2. The Raman spectra of H_2O_2-treating **1** and $\{V_{3.5}Nb_{24}\}$ exhibit a new peak at 868 cm^{-1} and 871 cm^{-1}, respectively, which are assigned to O-O stretch.

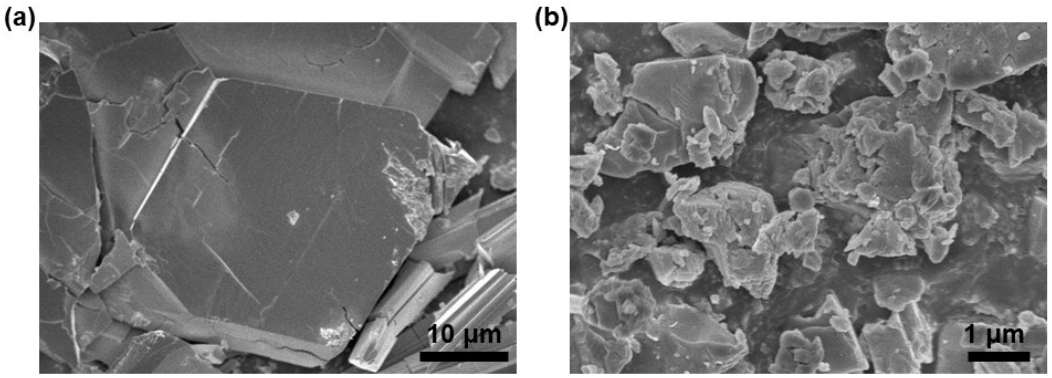

Fig. S21. Scanning electron microscopy (SEM) images of $\{V_5Nb_{23}\}$ before (a) and after (b) catalytic reaction, indicating the decrease of crystallinity of the recycled catalyst.

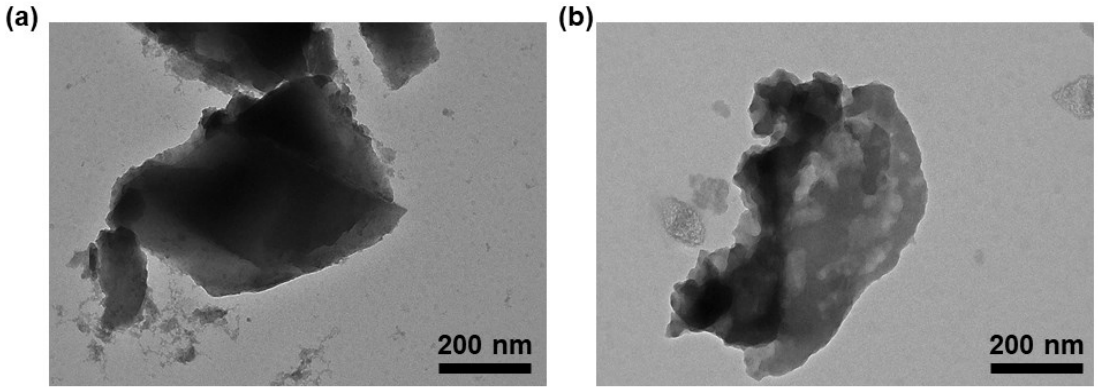

Fig. S22. High Resolution Transmission Electron Microscope (HRTEM) images of $\{V_5Nb_{23}\}$ before (a) and after (b) catalytic reaction.

References

1 M. Filowitz, R. K. C. Ho, W. G. Klemperer and W. Shum. *Inorg. Chem.*, 1979, **18**, 93.

2 G. M. Sheldrick, *SHELXL 97 Program for Crystal Structure Refinement*, University of Göttingen, Göttingen, 1997.

3 G. M. Sheldrick, *Acta Crystallogr., Sect. A*, 2008, **64**, 112.

4 Bruker AXS GmbH, *SHELXTL v6.14*, Bruker Analytical X-Ray Systems Inc., Madison, 2014.

5 J. Dong, H. J. Lv, X. R. Sun, Y. Wang, Y. M. Ni, B. Zou, N. Zhang, A. X. Yin, Y. N. Chi and C. W. Hu, *Chem. Eur. J.*, 2018, **24**, 19208.

6 C. Bisio, F. Carniato, C. Palumbo, S. L. Safronyuk, M. F. Starodub, A. M. Katsev, L. Marchese and M. Guidotti, *Catal. Today*, 2016, **277**, 192.

7 R. D. Gall, C. L. Hill, J. E. Walker. *Chem. Mater.*, 1996, **8**, 2523.

8 Y. J. Hou, H. Y. An, Y. M. Zhang, T. Hu, W. Yang and S. Z. Chang, *ACS Catal.*, 2018, ***8***, 6062.

9 F. Carniato, C. Bisio, R. Psaro, L. Marchese and M. Guidotti, *Angew. Chem. Int. Ed.*, 2014, **53**, 10095.

10 C. T. Buru, P. Li, B. L. Mehdi, A. Dohnalkova, A. E. Platero-Prats, N. D. Browning, K. W. Chapman, J. T. Hupp, and O. K. Farha, *Chem. Mater.*, 2017, **29**, 5174.

11 S. R. Livingston and C. C. Landry, *J. Am. Chem. Soc.*, 2008, **130**, 13214.

12 L. Jin, Z. K. Zhu, Y. L. Wu, Y. J. Qi, X. X. Li and S. T. Zheng, *Angew. Chem. Int. Ed.*, 2017, **56**, 16288.

13 Y. B. Liu, J.H. Yu, J. Liu, Y. K. Lu, J. Q. Xu and T. G. Wang, *J. Mol. Struct.*, 2007, **833**, 58.

14 X. S. Zang, H. Q. Tan, Q. Wu, Y. Li, Y.G. Li and E. B. Wang, *Inorg. Chem. Commun.*, 2010, **13**, 471.

15 T. H. Hu, Q. Wang, W. S. You, D. W. Song, C. Y. Huang, Y. Xu and Z. G. Sun, *Inorg. Chem. Commun.*, 2008, **11**, 470.

16 L. R. Zhang, Z. Shi, G. Y. Yang, X. M. Chen and S. H. Feng, *J. Chem. Soc., Dalton Trans.*, 2000, 275.

17 R. P. Bontchev and M. Nyman, *Angew. Chem. Int. Ed.*, 2006, **45**, 6670.